Journal of Corrosion Science Sciety of Korea
Vol. 9, 4, Dec., 1980

<研究論文>

Corrosion and Erosion Related to the In Situ Processing of Tar Sands

M. H. Swain and K. K. Orr*

Materials Div., Dep't of Mechanical Engineering, College of Engineering, University of Wyoming Laramie, WY82071, U. S. A.

Abstract

Bitumen-rich product was extracted from tar sands which were mined at Vernal, Utah. Various metals and limited number of ceramic coupons were installed at the steam drive extraction chamber. Under the hostile atmosphere the corrosion and erosion behavior of the coupons were charaterized using an optical microscope, a scanning electron microscope and a scanning Auger microscope.

초 록

농도가 진한 Bitumen 축출을 Vernal, Utah에서 채광한 Tar Sands에서 steam을 이용하는 과정에서, 여러가지 금속과 몇개의 요업체의 coupon의 corrosion과 erosion의 현상을 OM, SEM, SAM을 가지고 연구했다.

Ⅰ. Introduction

A materials test chamber was attached to the product line of the laboratory tar sand processing experiment being conducted by Dr. Hal Hutchinson at he Northsite Laramie, Wyoming under DOE contract #DE-AS20-79LC01761 Task 29. Various metals commonly used in pipes and valves were exposed to flowing and stationary bitumen-rich product from the steam drive experiment. Corrosion and erosion damage was examined on these materials after exposure to various conditions of time, temperature, and pressure.

Results indicate that the ceramic materials tested showed some accumulation of product but no deradation of the surface. Of the metallic alloys, the stainless steels, as a group, were most resistant. Bethlehem Steel alloys A36, RQC100, X70, and 729 also showed better resistance than the more common carbon and alloy steels. Of this latter group the resistance to this environment was best for AISI 8620 and decreased through AISI 4140, AISI 1045, and AISI 1020. These conclusions are based on weight gain, optical microscopy and SEM data, and Auger data.

* Present address: Department of Inorganic Materials Engineering, Hanyang University, Seoul, Korea

Ⅱ. Experimental Procedure

Ⅱ.1 Specimen Chamber

The specimen chamber was designed of ASTMA283 pressure vessel steel to withstand a hydrostatic pressure of 1000 psi at room temperature. Operating conditions for the tar sand steam drive experiment would not exceed 350 psi at 500°F. Schematics of the chamber are shown in Figures 1, 2, and 3. Figure 4 shows how the specimen chamber is intergrated into the tar sand processing apparatus. Features of the materials chamber include:

°Inlet nozzle to increase product velocity to approximately 70fps. The product strikes the twelve corrosion/erosion samples mounted on the opposite wall at normal incidence.

°Large removable flange to permit access to samples

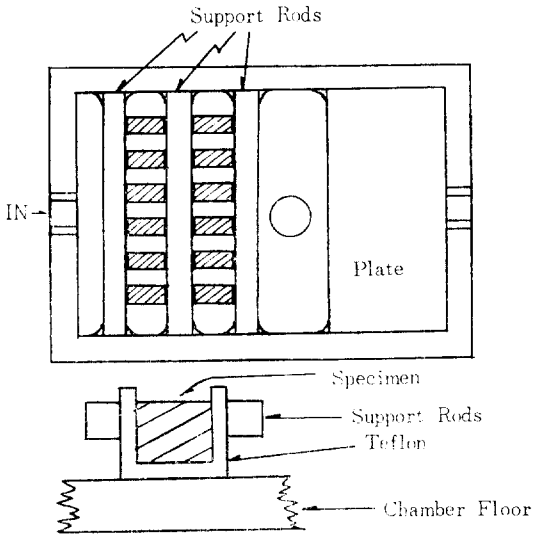

Figure 1. Corrosion Specimen Fixture

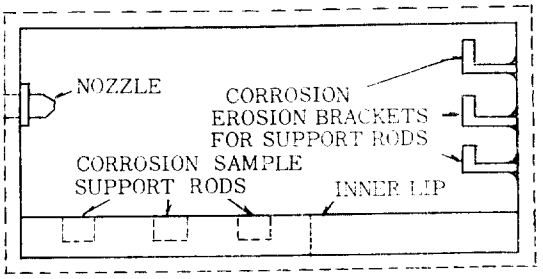

Figure 2. Side View of Specimen Chamber

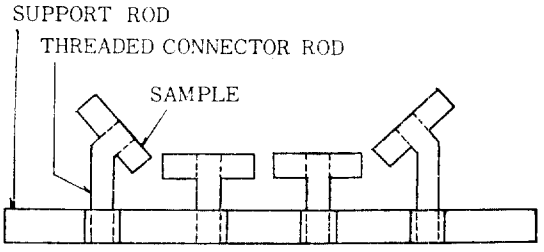

Figure 3. Top View of One Erosion/Corrosion Support Rod with Samples Mounted.

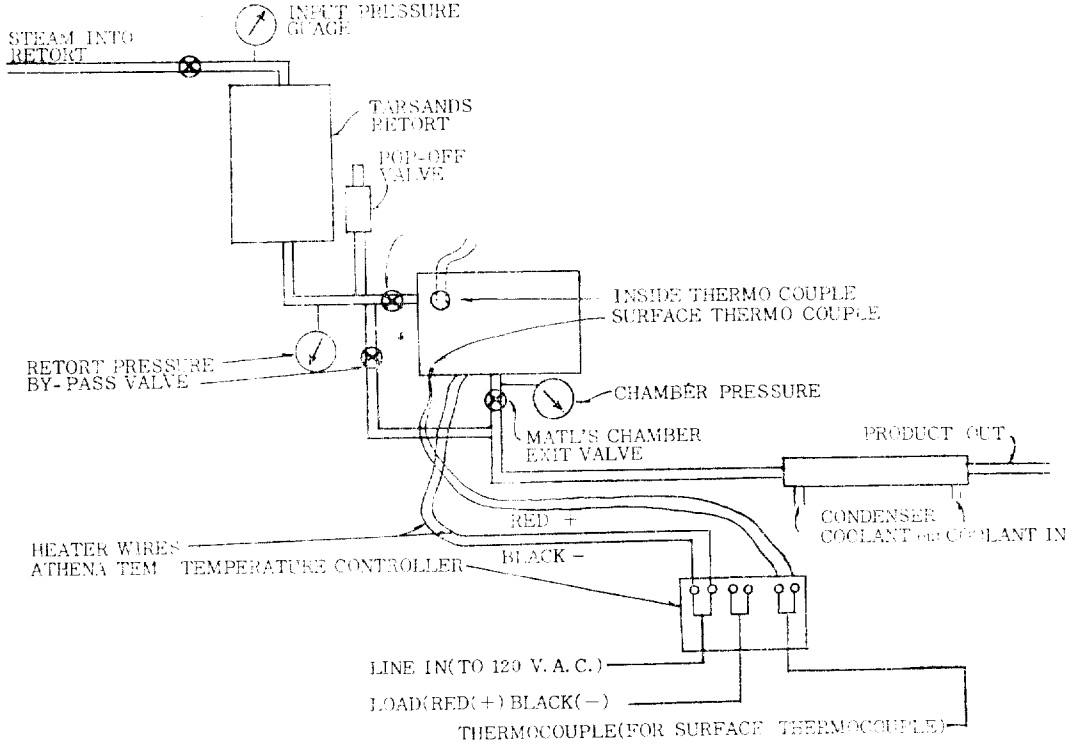

Figure 4. Tar Sand Processing Apparatus

without removing the entire specimen chamber from the system.

°An internal thermocouple to monitor chamber temperature.

°External heaters and thermocouple to maintain the desired chamber temperature. The chamber is heated while the retort is pressurized and thereafter no current input was necessary to maintain the temperature.

°Sample fixturing in the chamber bottom expose additional samples to the processing environment at a zero velocity, i.e., corrosion potential only.

°Pressure gages upstream and downstream of the nozzle permt calculation of the pressure drop on which the product velocity depends. Adjustment of the exit valve controls the outlet pressure and hence the pressure drop and nozzle velocity.

°A loop of stainless steel tubing with appropriate valving to permit the materials chamber to be bypassed without interrupting the experiment.

2.2 Materials Tested

The purpose of this project was to characterize material erosion/corrosion behavior in a simulated in-situ tar sands steam recovery environment, and, based on this characterization, to recommend the least costly materials system for well pipe and above ground support systems (e.g., piping, valves, fittings). The rational behind selecting materials for testing was to choose materials which fall into one or more of the following categories:

low to moderate cost,

commercially available,

historically developed for and used in the oil refining industry, and, which cover a reasonable spectrum of corrosion/erosion resistance.

Materials tested included:

°Carbon steels: AISI 1020, AISI 1045

°Alloy steels: AISI 4140, AISI 8620

Table 1. Compositions of Steels

Steel AISI	C	Mn	P	S	Si	Cr	Ni	Mo	Cu	Al	V	Cb	B
1045	.45	.90	.011	.022	—	—	—	—	—	—	—	—	—
1020	.18-.23	.30-.60	.040 max	.050 max	.25	—	—	—	—	—	—	—	—
8620	.18-.23	.70-.90	.040 max	.040 max	.20-.35	.40-.60	.40-.70	.15-.25	—	—	—	—	—
4140	.38-.43	.75-1.00	.040 max	.040 max	.20-.35	.80-1.10	—	.15-.25	—	—	—	—	—
RS90*	.31	.51	.004	.029	.28	1.12	.07	.20	.10	—	—	—	—
K55**	.42	1.06	.016	.034	.22	.03	.02	.01	.01	—	—	—	—
A36	.21	1.06	.010	.032	.26	—	—	—	—	.047	—	—	—
729	.13	1.37	.013	.004	.37	—	—	—	—	.036	—	—	—
X70	.13	1.34	.017	.011	.25	—	—	—	—	.057	0.56	0.36	—
RQC100	.17	1.48	.012	.018	.25	—	—	—	—	.045	—	—	.003
304	.08 max	2.0	.045 max	.030 max		18.5	9.5	—	—	—	—	—	—
310	.25 max	2.0	.045 max	.030 max	1.5	25.0	20.0	—	—	—	—	—	—
430	.12 max	1.0	.040 max	0.30 max	1.0	17.0	—	—	—	—	—	—	—
444L	.60	1.0	.040 max	.030 max	1.0	17.0	—	.75	—	—	—	—	—

*Similar to AISI 4140

**Similar to AISI 1040

°Republic steels: RS90, K55

°Bethlehe m steels: X70, A36, 729 RQC100

°Stainless steels: Types 304, 310, 430, 444L

Normal compositions of these metals are given in Table 1.

The materials from Bethlehem Steel and Republic Steel are modifications of alloys developed in part for oil field applications. RQC 100 is avilable in plate form only at this time.

2. 3 Sample Preparation

With the exception of the RS90 and K55 alloys which came in pipe sections, plates of each material 1/4 to 1/2 inch thick were used to make the test samples. Square coupons one inch on a side were cut using a cut off wheel. Samples to be mounted on the chamcer side for corrosion/erosion studies were tapped so that they could be threaded onto the support bars.

Rough polishing through 400 grit silicon carbide paper was accomplished on a belt sander. Fine polishing included 600 grit paper and 5 micron and 1 micron aluminum oxide powder on a wet polishing wheel. The polished surface was preserved until testing with a light coating of oil. Samples for the chamber side were polished on one surface only. Samples for the chamber bottom were polished on both large surfaces.

Optical study of the microstrucures of each alloy was accomplished by etching a polished sample in 2% nitanol and viewing in a Zeiss optical microscope. These samples were fine polished again to a smooth surface before use as test samples.

III. Results

III. 1 Microstructure

Using a Zeiss optical microscope, micrographs were taken of a polished and etched sample of each alloy. Figures 5 through 10 are representative views of the 500X. In general the grain size is quite small leading to the rather mottled appearance of the microsturctures different microstructures taken at a magnification of at this magnification. Note the light regions in the darker matrix visible most readily in Figures 6 and 9. These are ferrite grains, the first transformation product in the cooling of a hypoeutectoid steel from the austenizing temperature, and indicate the position of the prior austenite grain boundaries.

III. 2 Materials Tested

Tables 2 through 7 list the sample coupons tested in each of the six steam drive experiments for which the materials chamber was involved. The position of each

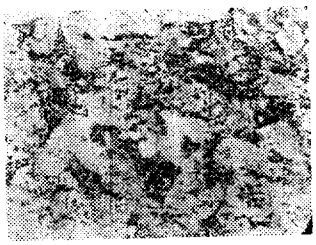

Figure 5. Microstructure of AISI 1020. 500X.

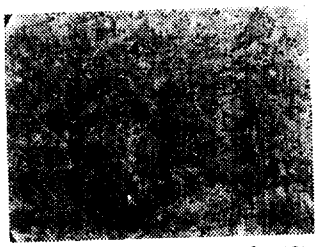

Figure 6. Microstructure of AISI 1045. 500X.

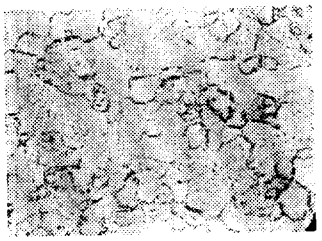

Figure 7. Microstructure of AISI 4140. 500X.

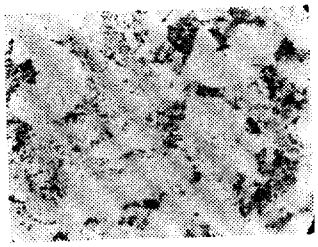

Figure 8. Microstructure of AISI 8620. 500X

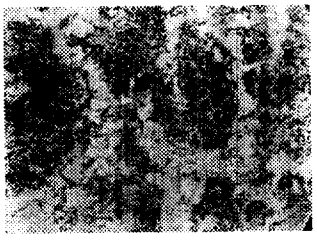

Figure 9. Microstructure of K55. 500. X

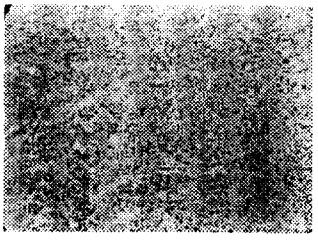

Figure 10. Microstructure of RS90. 500X.

sample at the side or bottom of the chamber is given along with an indication of prior runs for which the same coupon was used. Multiple exposures were used, with interim examinations, to build up longer total exposure times.

Runs 1, 2, and 3 are part of the data used by Kevin Watts for his thesis[1] as Runs 6, 10, and 12. The operating parameters were determined by him. For the first run an exit valve from the materials chamber one inch above the chamber floor was used. Most of the heavy oil which is the initial product was trapped in this one-inch layer around the corrosion samples throughout the test and Watts was not able to get accurate data on product quantity and composition as a function of time. For this reason all subsequent tests were made using the drain outlet at the chamber bottom as the product exit.

Runs 4, 5, and 6 are not part of Watts' thesis but were made solely for the benefit of the materials research project. The run times for 4 and 5 were increased to 16 hrs each in order to achieve longer total exposure times. Runs 5 and 6 inovlved the generally more corrosion resistant steels and stainless steels and hence longer times were necessary to achieve measurable surface changes.

III. 3 Weight Change

Table 8 gives the net change in sample weight of the carbon and alloy steel coupons exposed for 16 or 24 hours in runs 1, 2, and 3. Whether the sample was located on the chamber side(s) or bottom(b) is also indicated. A positive value for weight change indicates a weight gain whereas a negative value indicates a weight loss. In several instances an average weight loss rate for a given material in the side or bottom positions has een calculated. Weight loss measurements taken after Run #4 for RQC 100, X70 and A36 are also given since only one coupon of each of these materials was tested in the early runs. Note that the weight loss for each of these samples is approximately

Table 2 Run #1 (Run #6 in Watts' Thesis (1))
t=8 hours. T_{Box}=325°F
P_{Box}=150 psi (ave). $\triangle P_{Box}$~10 psi
Flow Rate of Steam=6.0lbm/hr
Steam Quality=55% T_{steam}=450°F

Samples	Side	Bottom
AISI 8620	4	2
AISI 1045	2	2
AISI 1020	0	2
AISI 4140	4	2
RS90	0	2
K55	0	2

Table 3 Run #2 (Run #10 in Watts' Thesis)
t=8hours. T_{Box}=350°F, P_{Box}=140psi (ave)
$\triangle P$~40psi. Flow Rate of Steam=2.1lbm/hr
Steam Quality=90%. T_{steam}=350°F

Samples	Side	Bottom
AISI 8620	2^+	2^+
AISI 1045	1^+	2^+
AISI 1020	2*	2^+
AISI 4140	2^+, 1*	2^+
RS90	2*	2^+
K55	2*	2^+
A36	0	1*
X70	0	1*
RQC100	0	1*

$^+$ Samples from run #1, cleaned ultrasonically and returned to original position. Total exposure of 16 hours after this run
* New samples

Table 4 Run #3 (Run #12 in Watts' Thesis)
t=7.5**. T_{Box}=350°F, P_{Box}=170psi
Flow Rate of Steam=2.3lbm/hr
Steam Quality=90%. T_{steam}=400°F

Samples	Side	Bottom
AISI 8620	2^+	2^-
AISI 1045	1^+	2^+
AISI 1020	2*	2^-
AISI 4140	2^+, 1*	2^+
RS90	2*	2^+
K55	2*	2^+
RQC100	0	1*
X70	0	1*
A36	0	1*

$^+$ 23.5 hours exposure (Runs1, 2, 3)
* 15.5 hours exposure (Runs2, 3)
** Pressure gradually dropped during last two hours as retort tube plugged with product. Test was terminated after 7.7 hosur

Table 5 Run #4 (Not included in Watts' Thesis)
t=16hours
T_{Box}=415°F T_{steam}=425°F P_{Box}=330psi

Samples	Side	Bottom
AISI 8620	2+	2+
AISI 1045	1+	2+
AISI 1020	2*	2+
AISI 4140	2+, 1*	2+
RS 90	2*	2+
K 55	2*	2+
RQC 100	0	1*
X 70	0	1*
A36	0	1*

+ 39.5 hours exposure (Runs 1, 2, 3, 4)
* 31.5 hours exposure (Runs 2, 3, 4)

Table 6 Run #5 (Not included in Watts' Thesis)
t=16hours
T_{Box}=420°F T_{steam}=425° P_{Box}=325psi

Samples	Side	Bottom
AISI 8620	0	0
AISI 1045	0	0
AISI 1020	0	0
AISI 4140	0	0
RS 90	0	1
K 55	0	1
RQC 100	2	3
X 70	2	0
A 36	1	2
729	2	1
Type 304	0	1
Type 310	4	2
Type 430	0	1
Type 444L	0	1
Alumina Ceramics & Harbide*		6

* Harbison Walker Refractories Co.

doubled when exposure time increases from 16 to 32 hours.

Table 9 gives the net change in sample weight of the alloy and stainless steels and ceramic coupons tested in Runs 5 and 6. The information parallels thatgiven in Table 8. No data is available for three samples due to an error in recording the initial weights.

Table 7 Run #6 (Not included in Watts' Thesis)
t=8hours T_{Box}=415°F. T_{steam}=425°F
P_{Box}=325psi

Samples	Side	Bottom
AISI 8620	0	0
AISI 1045	0	0
AISI 1020	0	0
AISI 4140	0	0
RS 90	0	1
K 55	0	1
RQC 100	2	3
X 70	1	0
A 36	1	2
729	2	1
Type 304	1+	1
Type 310	2	2
Type 430	1+	1
Type 444L	1+	1
Alumina Refractories & Harbide		6

+ Exposed in run #6 only. All others were in same position for Run #5

III. 4 Optical and Scanning Electron Microscope Study of Sample Surface Morphology

Figure 11 shows a typical polished surface of a sample at 500X prior to exposure in the tar sand processing environment. Note that the surface is smooth with tiny spots due to dust in the microscope lens system. These spots are present on all of the optical photos in the same pattern. Figure 12 on the other hand illustrates the type of surface scratches developed during rough polishing. The finer scratches are due to 400 grit paper and the larger ones are from a much coarser grit. The features in these two micrographs should not be confused with the erosion or corrosion damage features on many of the materials after exposure.

Figures 13 through 18 were taken of samples from the chamber floor after Run #1. As mentioned in section III. 2., these samples were surrounded by heavy oil product during the first eight hour run, rather than exposed to a mixture of water vapor and various product substances as was the case in the subsequent runs. The spots which were also visible on the polished surfaces are evident and some slight variation in reflectivity typical of a thin oxide or reaction product layer.

Table 8 Weight Change of Samples After Runs #3 and #4.

Metal	Sample Number	Position*	Run #3 Exposure Time (Hours)	Run #3 Weight Change (Grams)	Run #3 Averaged Rate of Weight Loss g/cm²hr	Run #4 Exposure Time (Hours)	Run #4 Weight Change (Grams)
AISI 8620	1	S	24	−.1091	.0006		
	2	B	24	−.0444	(S)		
	3	B	24	−.0042			
	4	S	24	−.0980			
AISI 1045	2	B	24	−.0110			
	3	S	24	−.0006			
	4	B	24	−.1482			
AISI 1020	1	S	16	−.9699	.0095		
	2	B	24	−.0057	(S)		
	3	S	16	−.9859			
	4	B	24	−.0050			
AISI 4140	3	B	24	+.0079	.0067		
	4	B	24	+.0028	(S)		
	5	S	24	−.5824			
	6	S	24	−.0055			
	7	S	16	−1.2815			
RS90	1	S	24	+.0701			
	2	S	24	−.0543			
	3	B	24	−.0069			
	4	B	24	−.0031			
K 55	1	B	24	−.0012			
	2	B	16	+.0051			
	4	S	24	−.9311			
	5	S	16	+.0099			
RQC 100	1	B	16	−.0047	.00003	32	−.0111
X 70	1	B	16	−.0090	(B)	32	−.0168
A 36	1	B	16	−.0051		32	−.0126

** Negative value=weight loss. Positive value=weight gain

* B (bottom) and S (side)

The coloration is related to the phase structure. This is most apparent when comparing AISI 8620 in Figure 15 with the microstructure shown in Figure 8.

Figures 19, 20, and 21 are typical views of three steels after exposure on the wall during Run #1. There is a slight increase in damage in these samples over those on the floor. It is seen in Figures 19 and 21 as bright patches indicating a thicker oxide or contamination layer.

At this point two steps must be taken: (1) the use of the SEM to obtain a clearer, indepth, view of the surface morphology, and (2) increased exposure times to allow for more accurate comparisons between materials.

Figures 22 through 34 are a series of scanning electron microscope(SEM) micrographs from several of the carbon and alloy steels from the chamber side after Run #4, or after 40 hours exposure. These samples have been cleaned ultrasonically in a sequence of methylene chloride, acetone, and ethanol baths to remove any loosely adhering oils of other products and expose the corrosion/erosion damage. Note the excellent contrast and depth of field produced in SEM micrographs as compared to the optical micrographs. In general the micrographs can be interpreted unambiguously by assuming they are reflected light images rather than elect-

Table 9 Weight Change of Samples in Runs #5 and/or #6

Metal	Sample Number	Position	Exposure Time (Hours)	Weight Change (Grams)
RS 90	1	B	24	(error)
K 55	1	B	24	+.0080
RQC 100	1	S	24	−.0466
	2	S	24	−.0840
	4	B	24	+.0044
	5	B	24	+.0056
	6	B	24	+.0064
X 70	2	S	24	−.0242
	3	S	16	−.0221
A 36	2	S	24	−.0293
	3	B	24	−.0036
	4	B	24	−.0018
729	1	S	24	−.0460
	2	S	24	−.0567
	3	B	24	+.0584
Type 304	1	B	24	+.0089
	4	S	8	−.0004
Type 310	1	B	24	+.0092
	2	B	24	+.0110
	3	S	24	+.0003
	4	S	16	+.0056
	5	S	24	(error)
	6	S	16	(error)
Type 430	1	B	24	+.−115
	3	S	8	+.0011
Type 444L	1	B	24	+.0130
	4	S	8	+.0027
Ceramics	1	B	24	+.5315
	2	B	24	+.5410
	3	B	24	+.6092
	5	B	24	+.1735
	6	B	24	+.3406
Carbide	4	B	24	+.3782

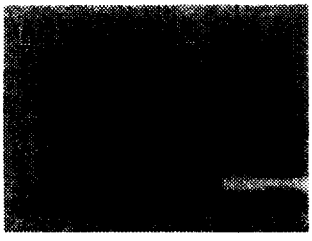

Figure 11. Surface of Polished Sample Prior to Test. 500X.

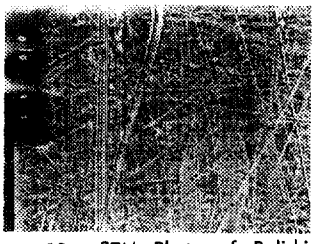

Figure 12. SEM Photo of Polishing Scratches on K55 Specimen. 100X.

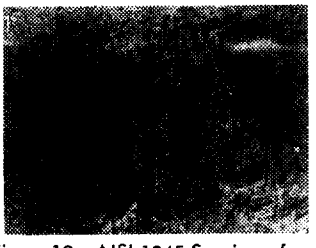

Figure 13. AISI 1045 Specimen from Bottomafter Run #1. 500X.

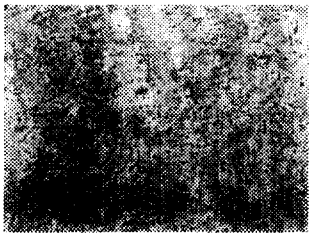

Figure 14. K55 Specimen from Bottom after Run #1. 500X.

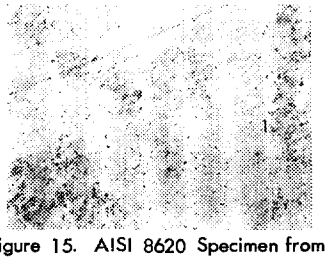

Figure 15. AISI 8620 Specimen from Bottom after Run #1. 500X.

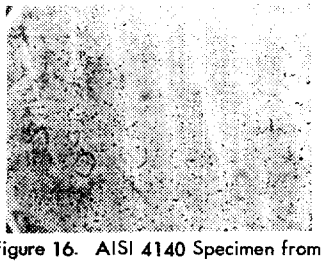

Figure 16. AISI 4140 Specimen from Bottom after Run #1. 500X.

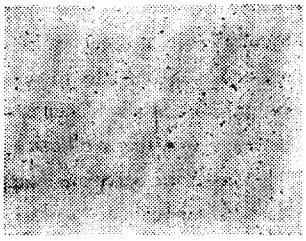

Figure 17. RS90 Specimen from Bottom after Run #1. 500X.

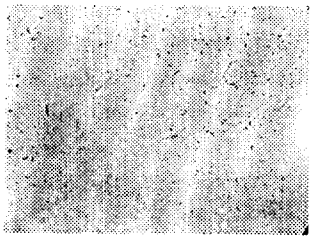

Figure 18. AISI 1020 Specimen from Bottom after Run #1. 500X.

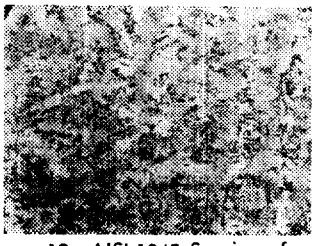

Figure 19. AISI 1045 Specimen from Side after Run #1. 500X.

Figure 20. AISI 4140 Specimen from Side after Run #1. 500X.

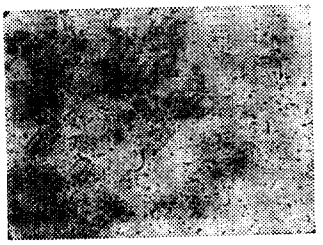

Figure 21. AISI 8620 Specimen from Side after Run #1. 500X.

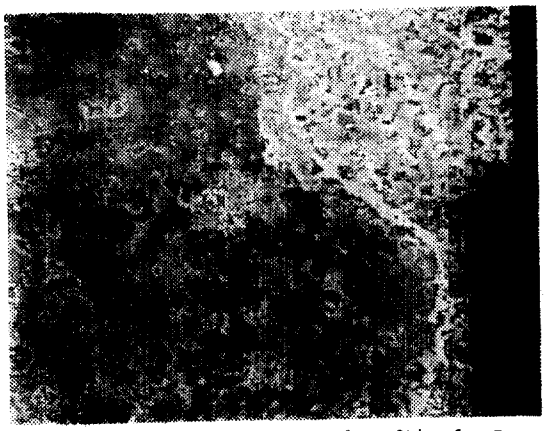

Figure 22. AISI 1020 Specimen from Side after Run #4. 200X.

Figure 23. AISI 1020 Specimen from Side after Run #4. 2000X.

ron images. Small dark areas are depressions in the surface or pits from which few electrons escape and a low signal intensity results. Bright areas are caused by sharp edges and small protruding particles from which electrons escape in all directions causing a high signal intensity. Bright areas or edges are also evidence of non-conducting particles or layers such as oxides or sulfides. In this case ferrous oxider and sulfides or silica (sand) particles from the retort embedded in the surface are likely sources of bright areas.

Figures 22 and 23 are typical views of A1S1 1020 steel after 40 hours of exposure to the tar sand processing environment. In the upper left corner of the picture the surface shading of the oxide is due to the microstructure. There are also patches where the oxide is thicker and jagged regions where the oxide has cracked and fallen away. The upper right hand regions show more severe damage. A thicker oxide with many more cracks and pits is present, Figure 23 is an enlargement from upper right of Figure 22 and shows considerable surface roughness. Close inspection reveals pitting or cracking occurring at a faster rate in some regions, probably along grain boundaries.

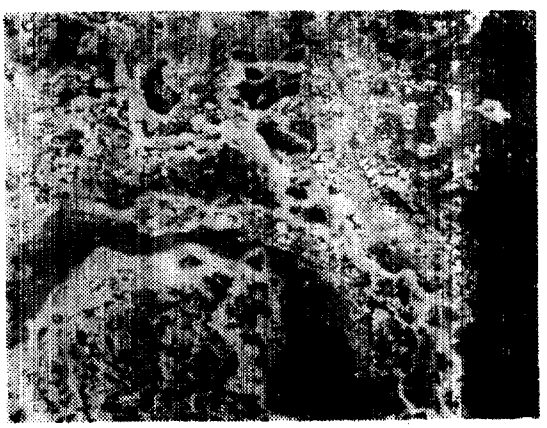

Figure 24. AISI 1045 Specimen from Side after Run #4. 200X.

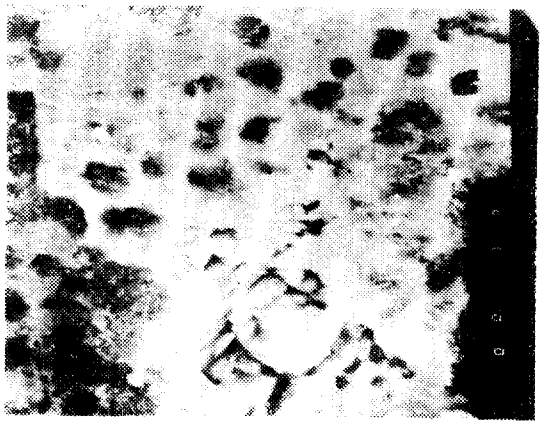

Figure 25. AISI 1045 Specimen from Side after Run #4. 2000X.

Figure 26. AISI 4140 Specimen from Side after Run #4. 200X.

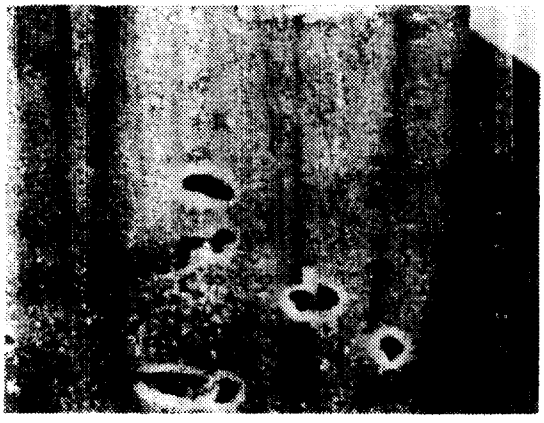

Figure 27. AISI 4140 Specimen from Side after Run #4. 500X.

Figure 28. AISI 8620 Specimen from Side after Run #4. 300X.

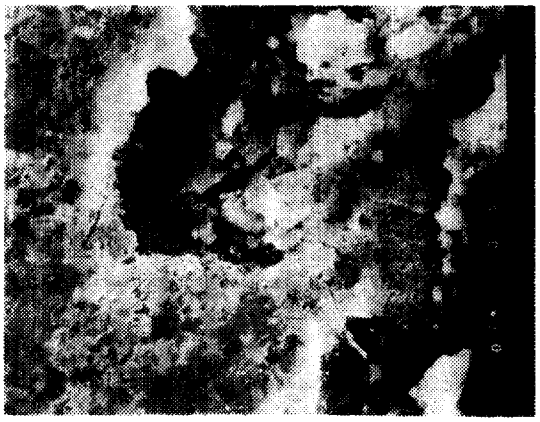

Figure 29. AISI 8620 Specimen from Side after Run #4. 1000X.

Figure 30. RS90 Specimen from Side after Run #4. 300X.

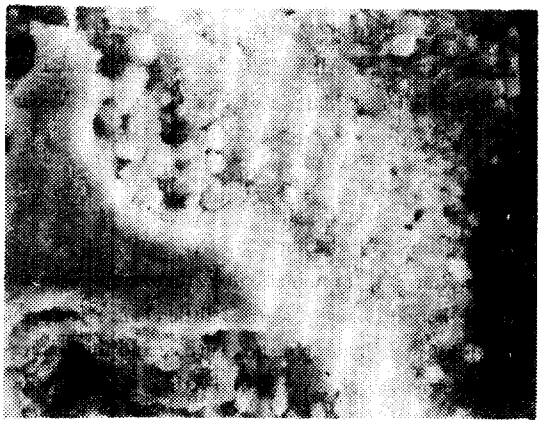

Figure 31. RS90 Specimen from Side after Run #4. 1000X.

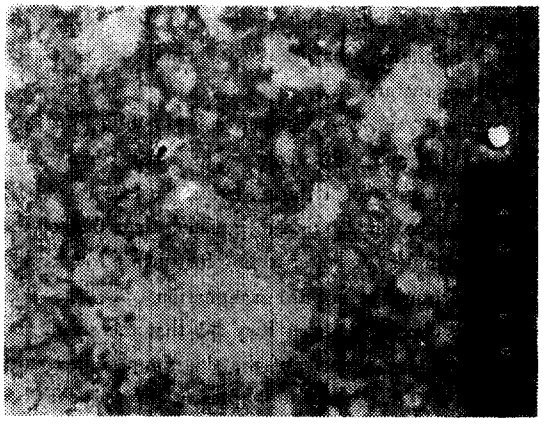

Figure 32. K55 Specimen from Side after Run #4. 100X.

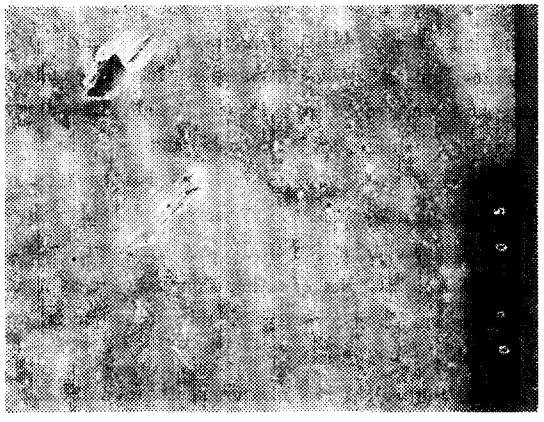

Figure 33. K55 Specimen from Side after Run #4. 300X.

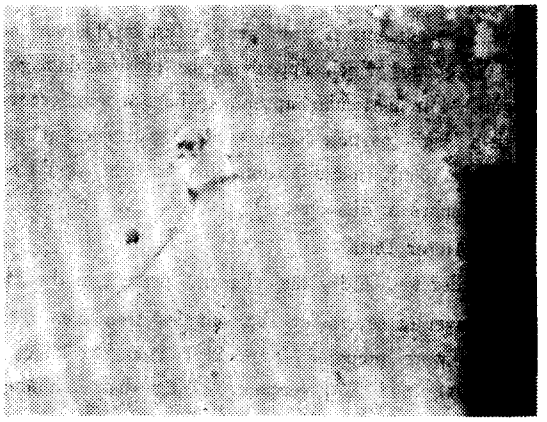

Figure 34. K55 Specimen from Side after Run #4. 1000X.

Figure 24 and 25 are of the AISI 1045 carbon steel. The oxide formation and peeling are evident here as well. Note the depth to which the surface has been removed in several local regions. Again a particular phase or location, such as a grain boundary, has undergone severe local attack.

Figures 26 and 27 are of the AISI 4140 alloy steel. Figure 26 shows large areas Which have a thin adherent oxide layer and small regions of more severe attack, i. e.a thicker oxide which begins to break away in patches.

Figures 28 and 29 are of the AISI 8620 alloy steel. As with AISI 4140 large arge areas show a thin adherent oxide and a smooth surface; patches of oxide cracking and local attack, though less severe than with the AISI 4140, are also evident. The parallel lines slightly off from the vertical are from sample polishing. Note that the regions of oxide peeling extend along the scratch direction. The surface layer was cold worked (plastically deformed) in this direction and the corrosion process as a result is also directional. Also as the oxide grows it may adhere more poorly in the scratches or grooves and popoff easily along this direction.

Figures 30 and 31 are of the RS 90 alloy. Its composition is similar to that of the AISI 4140 and the similarities are evident in the SEM photos. large smooth areas of thin adherent oxide are interspersed with regions of local attack.

Figures 32, 33, and 34 are of the K55 alloy whose composition is similar to that of AISI 1045. The corro-

sion layer is relatively thick but fewer regions of local attack are evident. A prominent feature on this surface are the gouges which appear to be erosion damage. Figure 34 in particular appears to have a long groove with a bright particle (perhaps SiO_2) embedded at one end. At 1000X magnification this particle would be .0005 inches in diameter.

3.5 Auger Data

In order to identify the elements present in the damage layer of several of the samples from Run #4, sections were prepared from AISI 4140, AISI 8620, RQC 100, and X70 coupons. Using their scanning Auguer microscope (SAM) a plot was made of the derivative of the electron signal with respect to electron energy vs energy in eV. Use of the derivative eliminates the large background secondary and backscattered electron signal and permits amplification of the Auger electron signal produced by each element present on the surface (0~100Å in depth) at its characteristic energies.

A typical SAM scan of the X70 alloy surface is shown in Figure 35. The peaks are labelled according to the element which produces the signal. While peak height is not directly proportional to percent concentration of each element, some correlation does exist. The predominent component as expected is iron oxide (Fe_3O_4). Smaller amounts of silicon, sulfur and carbon were also detected. The small carbon peak is a confirmation of our careful cleaning process prior to analysis. The source of sulfur is in part the alloy composition but also the tar sand bitumen. Silicon is probably present as SiO_2 particles from the tar sand.

Figure 36 is a scan of the same sample (X70) at the same spont after sputtering the surface with an inert gas (argon in this case). The sputtering removes the surface atoms layer by layer permittting a depth profiling of composition. After five minutes of sputtering a layer approximately 1000Å thick is removed. Relative changes between the scans in Figure 35 and 36 can be seen easily as the oxygen peaks have the same magnitude. The iron peaks are larger indicating a reduction of the oxide from Fe_2O_3 to a lower oxide such as Fe_3O_4, i.e., one containing a higher proportion of iron. Peaks for silicon, sulfur, and carbon are still present, indicating that these elements are not an adsorbed contaminant monolayer but an integral part of the surface corrosion layer.

Auger data from AISI 4140, AISI 8620, and RQC 100 are available at Materials Division, Dept of Mechanical Engineering, University of Wyoming.

4. Discussion

4.1. Runs #1 through #4

After Run #1, examination of the samples on the chamber bottom visually showed little change from the shiny gray metallic as-polished surface and this indicates the formation of a very thin oxide. This was due to the raised product exit which trapped the first product, the heavy oils, around these samples. It seemed to protect them from corrosion even at the elevated temperature. Samples of AlSl 8620 and Al Sl 4140 (Figures 15 and 16) show some thermal etching or temper coloration from the heat which delineates the microstrostructure.

Samples from the chamber side of of AlSl 1020, 1045, 4140, and 8620 show more distinct coloration and the presence of a thicker oxide. Surface roughness appears to be small, though greater than that of the bottom samples. A better feeling for surface roughening can be obtained from SEM examination.

It was concluded from Run #1 that the steam and oil mixture environment of the side samples was more severe than the heavy oils present in the chamber bottom. Therefore, there were no objections when Watts requested that chamber drain be used as the exit It was also concluded that most samples would need need exposure times greater than eight hours to give a good indication of behavior in this environment.

After Run #3, the 27 samples had accumulated exposure iimes of 16 to 24 hours. Weight change measurements, while showing considerable scatter, indicated several trends in erosion/corrosion behavior of the different alloys. Of the 27 samples, only six gained weight. These gains were all less than .01 grams, whereas weight losses of other samples were as much as 1.0 gram. The accuracy of this technique is probably about .005 grams.

Using the weight loss measurements for AlSl 1020, 4140, and 8620 samples on the chamber side, the following average weight loss rates were calculated:

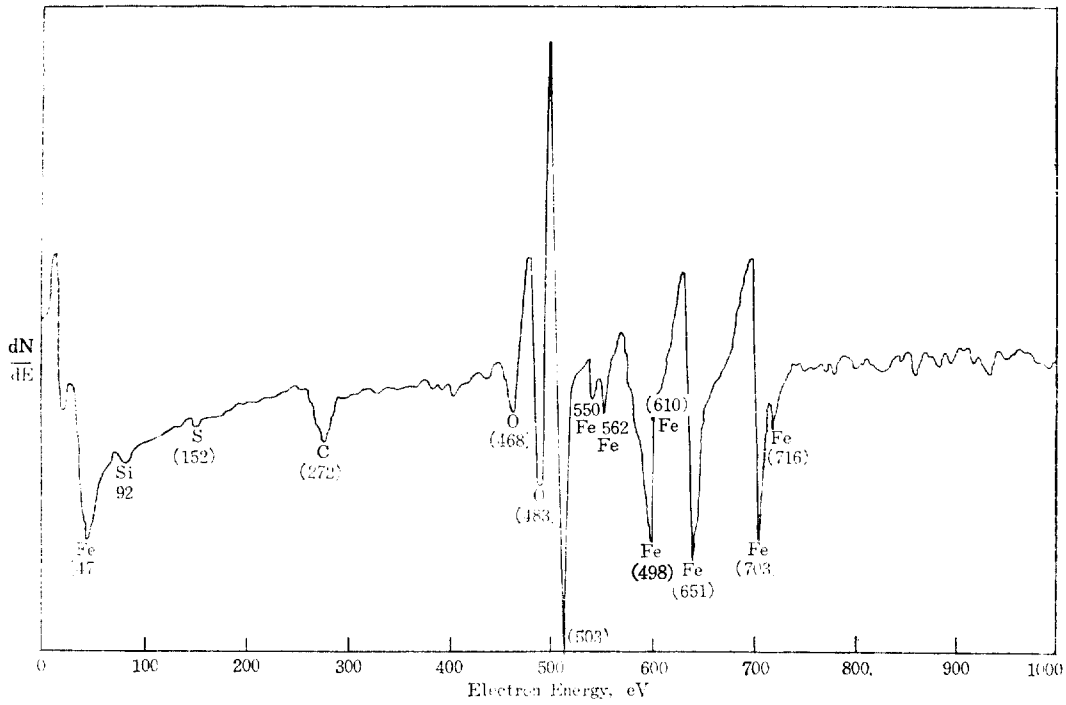

Figure. 35. Auger Scan of X70 Specimen Surace after Run #4

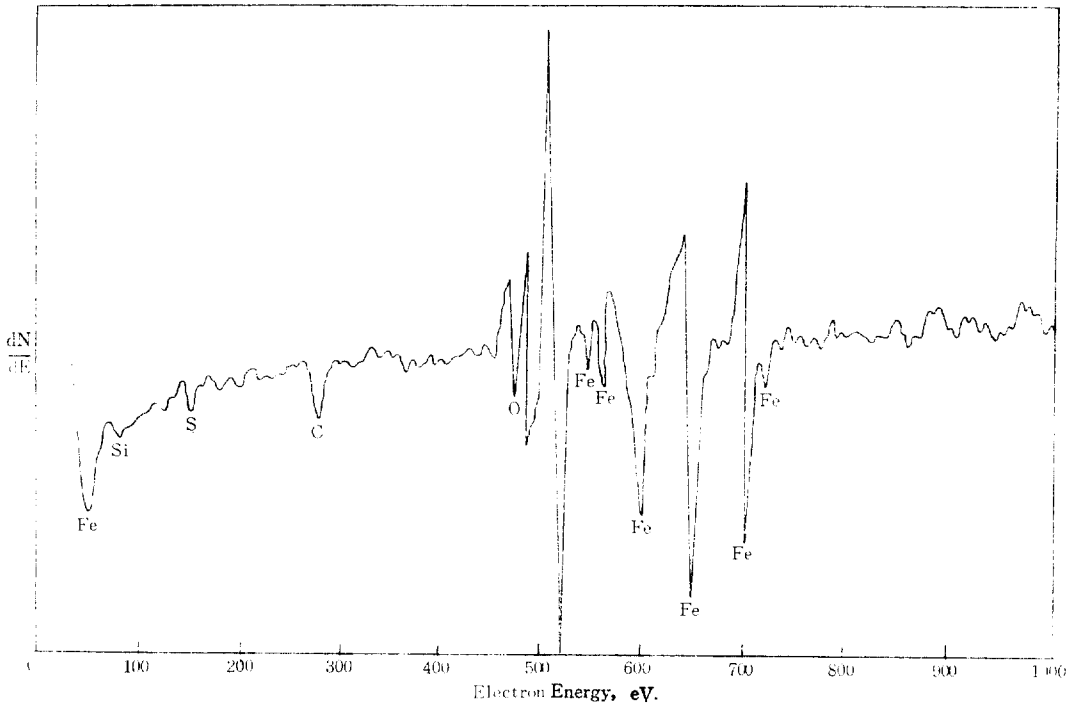

Figure 36. Auger Scan off Sputtered X70 Specimer after Run #4.

AlSl 1020	.0095g/cm²hr
AlSl 4140	.0067g/cm²hr
AlSl 8620	.0006g/cm²hr

From these rates it can be concluded that the erosion/corrosion resistance of AlSl 8620 is far superior to AlSl 1020 in this environment and considerably better than AlSl 4140. A larger data base would give more reliable rates than are possible here.

Data for RS90 and K55 were ambiguous with both weight losses and gains. The three Bethlehem steels RQC100, X70, and A36 all showed consistently good resistance. Weight loss rates were all much less than that for AlSl 8620 and averaged at .00003g/cm²hr for samples on the bottom in Runs #2 and 3. The weight change for these samples was checked again after Run #4 when the exposure time was 32 hours instead of 16 hours. The weight losses were all consistent with Run #3 measurements as all were approximately double. Even though only one sample of each material was tested, the consistency gives credence to the calculated weight loss rate. Visual examination of these samples after Runs #3 and 4 revealed shiny, metallic surfaces typical of a thin oxide and minimal pitting.

SEM micrographs of the first six materials of Table 8 bear out the above observations. AlSl 1020 (Figures 22 and 23) show heavy general oxidation and breaking away of the oxidized layers. This corresponds to the highest weight loss rate. Resistance improves as we progress through A1S1 1045, A1S1 4140, and A1S1 8620 (Figures 24 through 29). It is important to note that local pitting and grain boundary attack was clearly evident even in A1S1 8620. This would lead to little overall weight loss, but the presence of stress raisers at the grainboundaries can significantly degrade toughness and strength. It is important therefore to consider the surface damage mechanism shown by optical and SEM analysis as well as the easier weight change measurements.

Figures 32, 33, and 34 clearly indicate that erosion is part of the damage mechanism. While large particles can leave observable grooves and embedded particles, smaller particle impact was probably instrumental in initiating the oxide cracking and removal observed in all samples examined by SEM after Run #4.

Ⅳ. 2. Runs #5 and #6

Samples in Runs #5 and 6 included the Bethlehem steel and Republic Steel alloys, four stainless steels, and six ceramic materials. Weight change data is given in Table 9. Several trends are noted from this data. First, in comparison of stainless steels to the carbon and alloy steels, the weight change of the former group is generally much less.

For K55, RQC100, X70, 729, and 304 the samples on the side lost weight while those on the bottom gained. A possible mechanism is the oxidation of surface layers forming a thin adherent oxide and causing a weight gain. The oxidation rate of these materials is low because the dense, adherent oxide acts as a barrier to oxygen movement to the metal atoms underneath. The same materials on the side are struck by product droplets and sand particles. The impact fractures sections of the oxide which falls away, exposing fresh metal and causing a net weight loss. Theprocess continues in this cycle. The brittle oxide is of course more susceptible to impact loads than the tougher alloy.

The exceptions to this observation occur for A36 (all samples lost) and for 444L, 430, and 310 (all samples gained). For A36 the oxide formed may be more porous and less adherent. Volume expansion or contraction of the surface layers can cause interface stresses leading to spalling or cracking away of the oxide with no erosion process necessary. Data for 444L and 430 are for 8 hours only. The gains for these materials even for side samples can be explained by the formation of an oxide which is thinner than that for the K55, etc. group and therefore tough enough enough to remain intact and protective even under bombardment of the product stream. This is not unexpected since the oxide formed by these materials is very high in chromium (rather than iron) which is more protective and would have a different toughness (here assumed greater than Fe_2O_3).

Ⅳ 3. Auger Analysis

No significant differences between Auguer scans was noted for the alloys A1S1 4140, A1S1 8620, RQC100, and X70. (The scans are shown in Figures 35 and 36 and available data). In all cases the surface layer was primarily iron oxide (Fe_2O_3 and Fe_3O_4). Also dresent throughout at least the first 1000Å of each oxide were small quantities of silicon sulfur, and carbon. The

source of silicon is SiO_2 in the tar sand, and of car bon and sulfur is the bitumen product. Sulfur levels are not considered high enough to significantly alter the corrosion/erosion process. (Sulfur content of the bitumen from Asphalt Ridge tar sands is measured by Watts as 0.14% which is less than 3% of the sulfur content found in Athabasca tar sands (1)).

ACKNOWLEDGEMENT

This work supported by the U.S. Department of Energy under Contract DE AS20-79LCO1761.

REFERENCE

1. Watts, Kevin G., *Investihation of the Steam Flood Process for the AsphaltRidhe Tar Sands Deposit, Utah,* M.S., Department of Petroleum Engineering, University of Wyoming, 1979.